Supporting information

Catalytic oxidation properties of an acid-resistant cross-bridged cyclen Fe(II) complex. Influence of the rigid donor backbone and protonation on the reactivity.

Jean-Noël Rebilly, Christian Herrero, Katell Sénéchal-David, Régis Guillot, and Frédéric Banse

Materials and methods

Solvents and chemicals were of reagent grade and were distilled prior to use. H_2O_2 35% in water was used. Ligand cyclenCB-CH_2py (Chart 1) was synthesized according to a literature procedure.[1]

ESI mass spectrometry analyses were performed with a Bruker MicroTOFq spectrometer using a sodium formate calibrant. Solvents: Methanol HPLC LC/MS (Carlo-Erba), Acetonitrile HPLC (Carlo-Erba).

NMR spectra were recorded on Bruker 250 MHz, 300 MHz, and 360 MHz spectrometers.

Cyclic Voltammetry experiments were performed using an Autolab potentiostat and a conventional three electrode device (C working electrode, SCE reference electrode, Pt counter electrode). The electrolyte salt ($TBAPF_6$) was recrystallized and all the glassware was dried at 110°C before use. All cyclic voltammograms (CVs) were recorded under argon in acetonitrile solution containing 0.1 M Bu_4NPF_6 at a scan rate of 0.1 V/s at 20°C. All potential values are referred to SCE.

X-band EPR spectra were recorded on frozen solutions using a Bruker Elexsys 500E spectrometer equipped with a Bruker ER 4116DM X band resonator, an Oxford Instrument continuous flow ESR 900 cryostat, and an Oxford ITC 503 temperature control system. Conditions: Microwave frequency = 9.63 GHz, microwave power = 1.0 mW, modulation amplitude = 8 Gauss, modulation frequency = 100 KHz, gain = 50 db, temperature = 90 K. Spectral simulations were done using the Bruker software XSophe.

Stopped Flow absorption spectrophotometry was performed on a BioLogic SFM-4000 coupled to a J&M Tidas diode array spectrometer, with a two-syringe setup (one containing the iron complex, [Fe] = 2 mM, the other containing the oxidant). Experiments were at least triplicated for kinetic fits. Fits at 530 or 730 nm were performed using the BioKine software.

UV-visible. Electronic absorption spectra were recorded with a Varian Cary 60 spectrophotometer.

X-ray diffraction data for compound **[(cyclenCB-CH_2py)Fe^{II}(OTf)](OTf)** was collected by using a VENTURE PHOTON100 CMOS Bruker diffractometer with Micro-focus IuS source Cu Kα radiation. X-ray diffraction data for compound **[(cyclenCB-CH_2py)Fe^{III}(OMe)](OTf)$_2$** was collected by using a Kappa X8 APPEX II Bruker diffractometer with graphite-monochromated MoK_α radiation (λ = 0.71073 Å). Crystals were mounted on a CryoLoop (Hampton Research) with Paratone-N (Hampton Research) as cryoprotectant and then flash frozen in a nitrogen-gas stream at 200 K or 100 K. For compounds, the temperature of the crystal was maintained at the selected value by means of a 700 series Cryostream cooling device to within an accuracy of ±1 K. The data were corrected for Lorentz polarization, and absorption effects. The structures were solved by direct methods using SHELXS-97[2] and refined against F^2 by full-matrix least-squares techniques using SHELXL-2018[3] with anisotropic displacement parameters for all non-hydrogen atoms. Hydrogen atoms were located on a difference Fourier map

and introduced into the calculations as a riding model with isotropic thermal parameters. All calculations were performed by using the Crystal Structure crystallographic software package WINGX[4].

The crystal data collection and refinement parameters are given in Table S1.

CCDC 2184867-2184868 contains the supplementary crystallographic data for this paper. These data can be obtained free of charge from the Cambridge Crystallographic Data Centre and Fachinformationszentrum Karlsruhe via http://www.ccdc.cam.ac.uk/structures/.

***Table S1**. Crystallographic data and structure refinement details.*

Compound	**[(cyclenCB-CH_2py)Fe^{II}(OTf)](OTf)**	**[(cyclenCB-CH_2py)Fe^{III}(OMe)](OTf)$_2$**
CCDC	2184867	2184868
Empirical Formula	C_{18} H_{29} F_3 Fe N_5 O_3 S, C F_3 O_3 S	C_{18} H_{32} Fe N_5 O, 2(C F_3 O_3 S)
M_r	657.44	688.47
Crystal size, mm^3	0.07 x 0.22 x 0.24	0.01 x 0.12 x 0.17
Colour	yellow	green
Crystal system	monoclinic	monoclinic
Space group	*P* $2_1/c$	*P* $2_1/c$
a, Å	9.6666(4)	19.0222(9)
b, Å	14.8989(6)	12.1505(6)
c, Å	18.1683(8)	12.1044(5)
α, °	90	90
β, °	99.9130(10)	100.596(2)
γ, °	90	90
Cell volume, Å^3	2577.56(19)	2750.0(2)
Z ; Z’	4 ; 1	4 ; 1
T, K	100(1)	200 (1)
Radiation type ; wavelength Å	CuKα; 1.54178	MoKα ; 0.71073
F_{000}	1352	1420
μ, mm^{-1}	7.037	0.791
range, °	3.860 - 66.663	1.999 - 30.535
Reflection collected	36 732	62 137
Reflections unique	4 561	8 322
R_{int}	0.0433	0.0815
GOF	1.067	1.061
Refl. obs. (I>2(I))	4 421	4 707
Parameters ; restraints	354 ; 0	372 ; 0
wR_2 (all data)	0.0665	0.2354
R value (I>2(I))	0.0283	0.0743
Largest diff. peak and hole (e-.Å^{-3})	0.467 ; -0.349	1.753 ; -0.849

Table S2. Selected bond distances [Å] and angles [deg]:

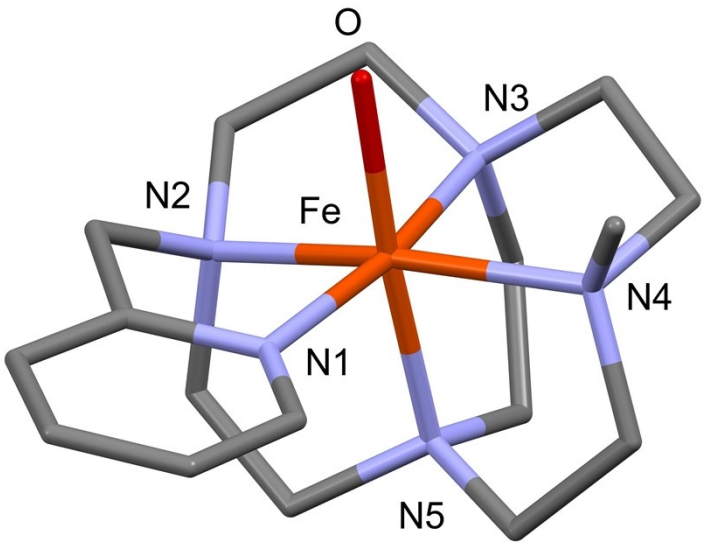

Compound / T(K)	**[(cyclenCB-CH_2py)Fe^{II}(OTf)](OTf)** **100K**	**[(cyclenCB-CH_2py)Fe^{III}(OMe)]$(OTf)_2$** **200K**
Fe-N(1)	2.1368(15)	1.997(3)
Fe-N(2)	2.2202(16)	1.999(3)
Fe-N(3)	2.1581(16)	1.958(3)
Fe-N(4)	2.1916(16)	2.047(3)
Fe-N(5)	2.1759(16)	1.998(3)
Fe-O	2.1121(13)	1.838(3)
N(1)-Fe-N(2)	78.53(6)	86.31(15)
N(1)-Fe-N(3)	156.27(6)	170.60(14)
N(1)-Fe-N(4)	120.38(6)	102.89(15)
N(1)-Fe-N(5)	98.31(6)	94.36(14)
N(1)-Fe-O	89.87(6)	90.65(14)
N(2)-Fe-N(3)	77.86(6)	84.67(14)
N(2)-Fe-N(4)	154.41(6)	165.66(14
N(2)-Fe-N(5)	81.67(6)	85.73(14)
N(2)-Fe-O	104.10(6)	95.54(14)
N(3)-Fe-N(4)	82.83(6)	86.47(14)
N(3)-Fe-N(5)	80.51(6)	87.62(13)
N(3)-Fe-O	93.64(6)	87.59(13)
N(4)-Fe-N(5)	78.70(6)	82.64(13)
N(4)-Fe-O	93.66(6)	95.34(13)
N(5)-Fe-O	170.85(6)	174.90(13)

All esds are estimated using the value of the full covariance matrix of least square.

Synthesis of complex **[(cyclenCB-CH_2py)Fe^{II}(OTf)](OTf)**

In a glovebox under Ar, cyclenCB-CH_2py (202 mg, 668 µmol) in 2 mL MeOH was added dropwise to a solution of $Fe^{II}OTf_2$ (236 mg, 668 µmol) in 3 mL MeOH. The resulting solution was stirred overnight. The volume was reduced to 2 mL and excess diethylether (20 mL) was added, resulting in the precipitation of a gum. After stirring overnight, the gum turned into a tan-yellowish powder that was filtered and washed with diethylether (331 mg, 75%). Crystals suitable for X-ray diffraction were obtained by slow diffusion of diethylether into a methanol solution of the complex in the glovebox.

Crystals of **[(cyclenCB-CH_2py)Fe^{III}(OMe)](OTf)$_2$**

Green crystals of **[(cyclenCB-CH_2py)Fe^{III}(OMe)](OTf)$_2$** suitable for X-ray diffraction were obtained by slow diffusion of diethylether into an aerated solution (exposed to air and kept on the bench in a schlenk for two weeks) of **[(cyclenCB-CH_2py)Fe^{II}(OTf)](OTf)** in methanol.

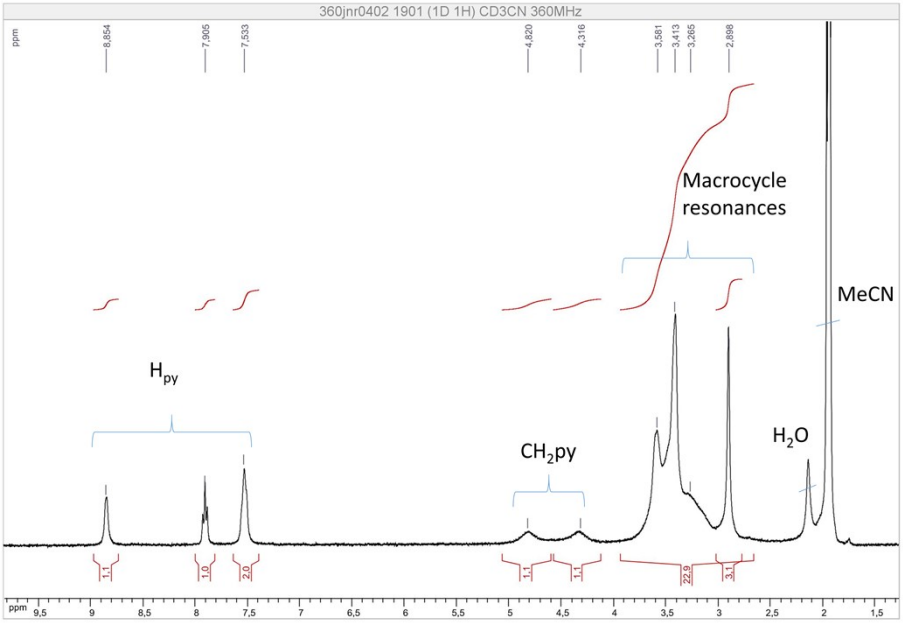

Figure S1. ^{1}H NMR spectrum (CD_3CN, 360 MHz, 300 K) of **[(cyclenCB-CH_2py)Fe^{II}(OTf)](OTf)**.

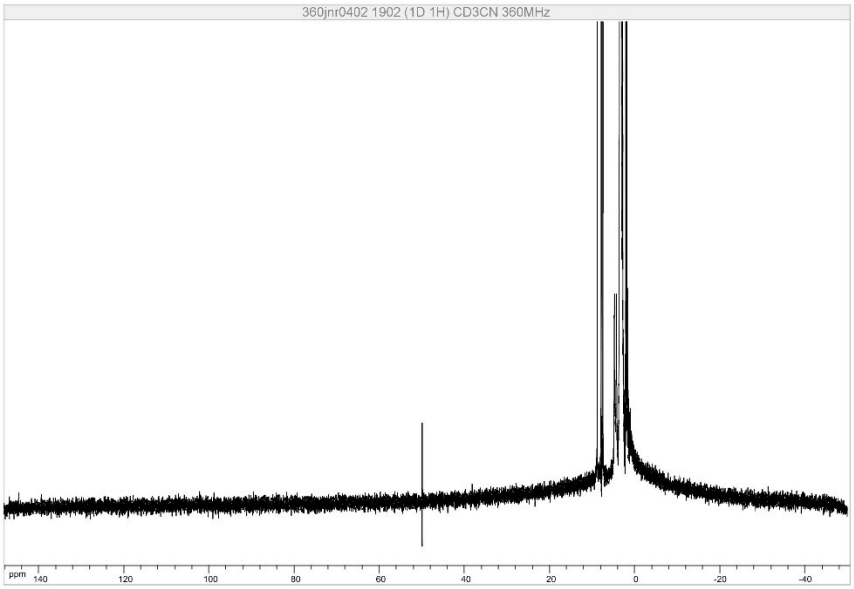

Figure S2. ^{1}H NMR spectrum (CD_3CN, 360 MHz, 300 K, wide spectral range) of **[(cyclenCB-CH_2py)Fe^{II}(OTf)](OTf)**.

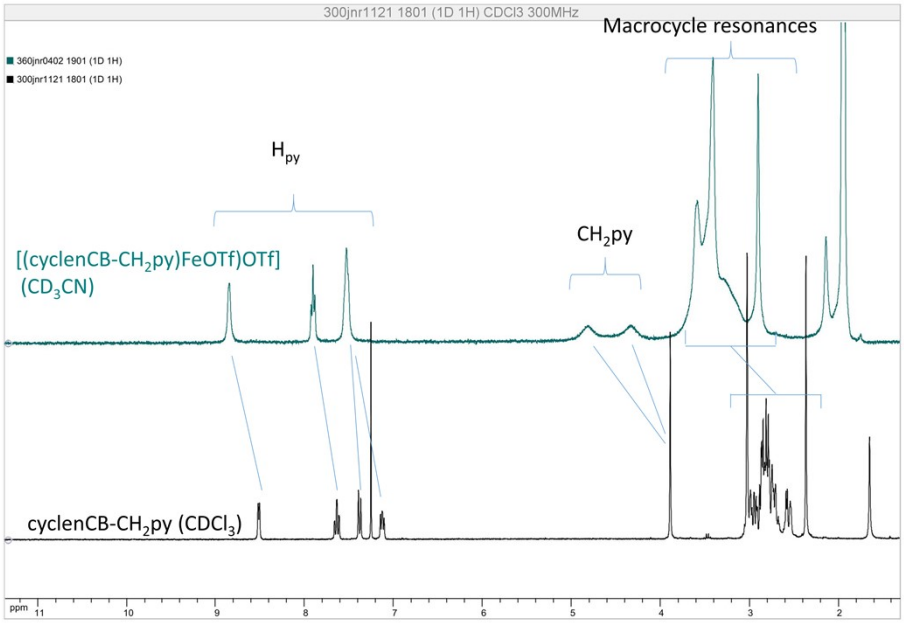

Figure S3. Comparison of the ^{1}H NMR spectra (300 K) of **[(cyclenCB-CH_2py)Fe^{II}(OTf)](OTf)** (360 MHz, CD_3CN) and **cyclenCB-CH_2py** (300 MHz, $CDCl_3$). The macrocycle and pyridyl resonances appear downfield shifted with respect to the ligand, in line with the pentadentate binding of cyclenCB-CH_2py observed in the solid state. The diamagnetic nature of the complex suggests that triflate has been substituted by acetonitrile in solution.

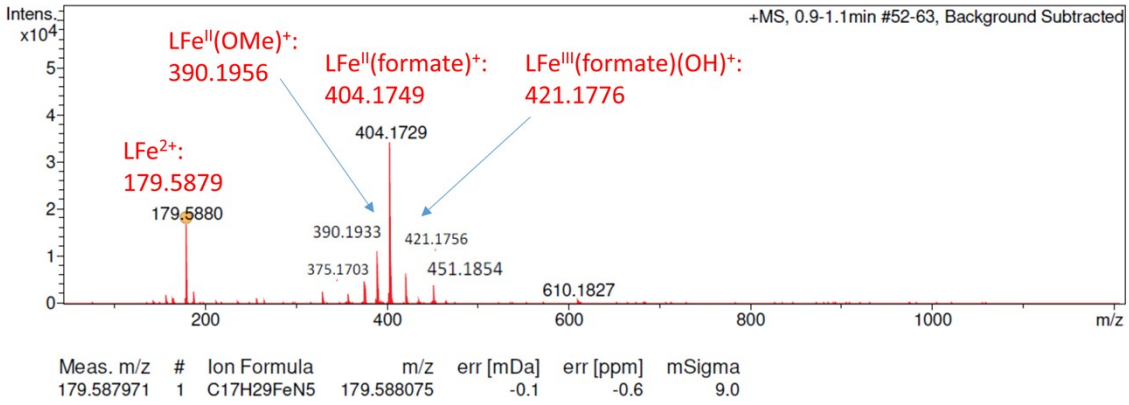

Figure S4. HR-ESI-MS spectrum of **[(cyclenCB-CH$_2$py)Fe^{II}(OTf)](OTf)**. m/z = 179.5880 (calcd. for [**(cyclenCB-CH$_2$py)**Fe^{II}]$^{2+}$: 179.5879, error = 0.6 ppm); m/z = 390.1933 (calcd. for [**(cyclenCB-CH$_2$py)**Fe^{II}(OMe)]$^{2+}$: 390.1956, error = 5.8 ppm); m/z = 404.1729 (calcd. for [**(cyclenCB-CH$_2$py)**Fe^{II}(formate)]$^{2+}$: 404.1749, error = 4.9 ppm); m/z = 421.1756 (calcd. for [**(cyclenCB-CH$_2$py)**Fe^{III}(formate)(OH)]$^{2+}$: 421.1776, error = 4.7 ppm). Formate was used as calibrant.

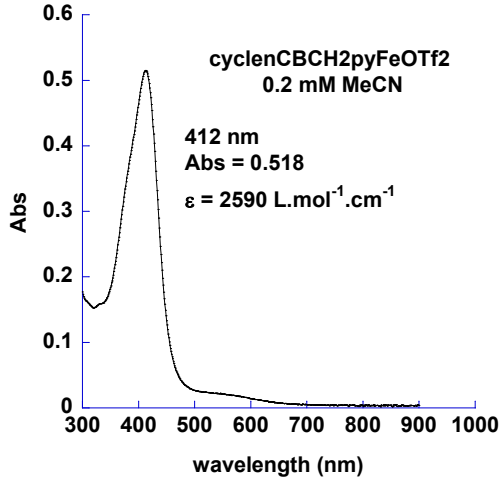

Figure S5. UV-vis spectrum of **[(cyclenCB-CH$_2$py)Fe^{II}(OTf)](OTf)**, 0.2 mM in MeCN (300 K).

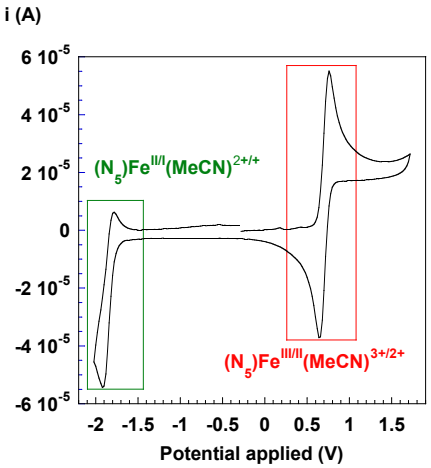

Figure S6. CV at a glassy carbon electrode of **[(cyclenCB-CH_2py)Fe^{II}(OTf)](OTf)** (C =2 mM) in MeCN (300 K). NBu_4PF_6 0.1 M. WE: GC, CE: Pt, Ref: SCE. Couple at $E_{1/2}$ = 0.71 V (ΔE = 100 mV) *vs* SCE is ascribed to a Fe^{III}/Fe^{II} couple and the less reversible one at $E_{1/2}$ = -1.84 V (ΔE = 130 mV) *vs* SCE is ascribed to a Fe^{II}/Fe^{I} couple.

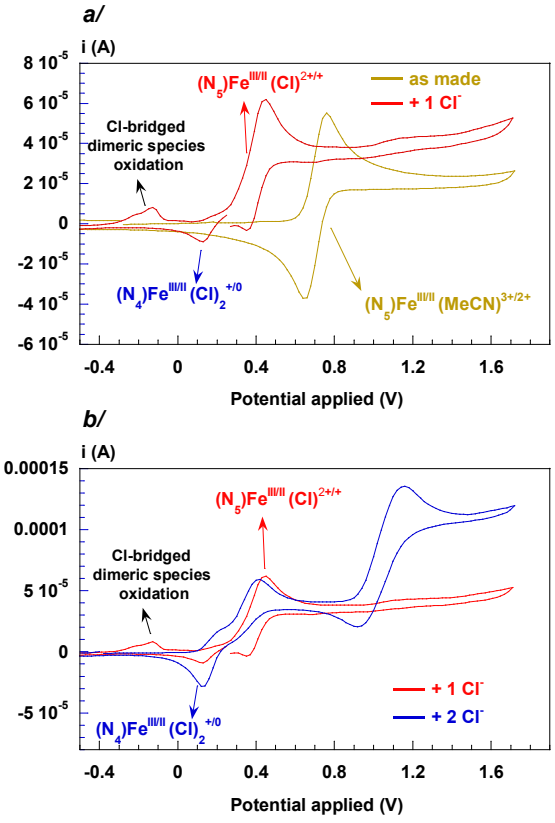

Figure S7. CVs at a glassy carbon electrode of **[(cyclenCB-CH_2py)Fe^{II}(OTf)](OTf)** (C =2 mM) in MeCN (300 K), before and after addition of a/ 1or b/ 2 equiv. NBu_4Cl. NBu_4PF_6 0.1 M. WE: GC, CE: Pt, Ref: SCE. The initial couple at $E_{1/2}$ = 0.71 V (ΔE = 100 mV) *vs* SCE is ascribed to a $(N_5)Fe^{III/II}(MeCN)^{3+/2+}$. After addition of 1 equiv. chloride, the couple at $E_{1/2}$ = 0.4 V (ΔE = 100 mV) is ascribed to $(N_5)Fe^{III/II}Cl^{2+/+}$. A weaker $(N_4)Fe^{III/II}Cl_2^{+/0}$ couple is detected at E_p^c = 0.12 V, along with the reoxidation of Cl-bridged dimeric species at E_p^c = -0.13 V. Upon addition of a 2nd equiv. chloride, the amount of $(N_4)Fe^{III/II}Cl_2^{+/0}$ couple increases and the oxidation of dimeric species vanished, in line with the displacement of equilibria towards $(N_4)Fe^{II}Cl_2$ in solution.

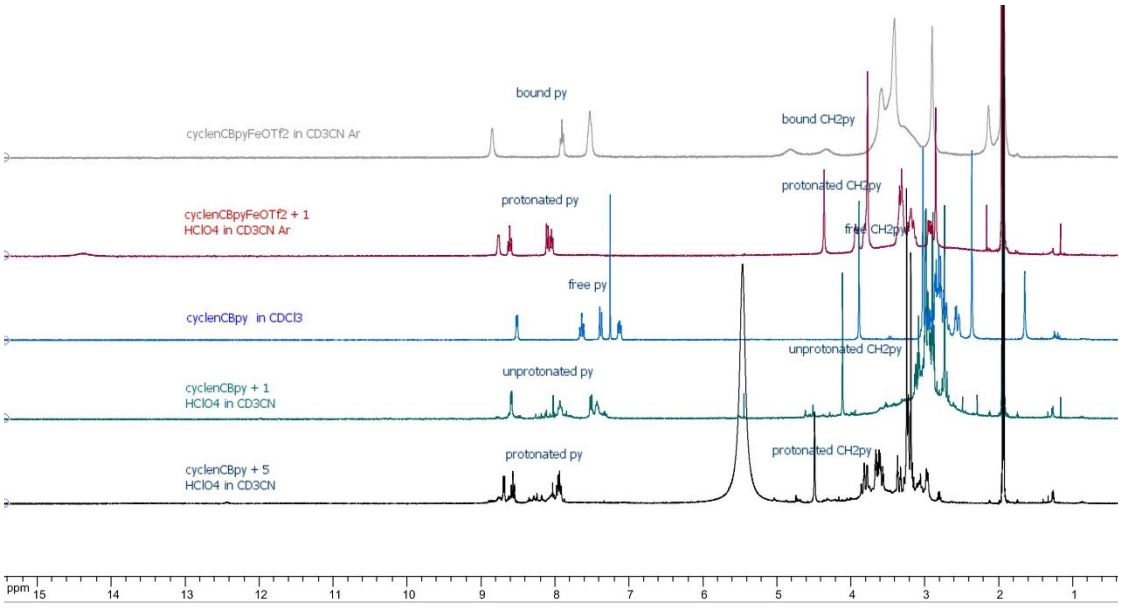

Figure S8. Comparison of the ^{1}H NMR spectrum (360 MHz, 300 K) of **[(cyclenCB-CH$_2$py)Fe^{II}(OTf)](OTf)** in the presence and absence of 1 equiv. $HClO_4$. For spectrum analysis purposes, the NMR spectra of **(cyclenCB-CH$_2$py)** ($CDCl_3$), and **(cyclenCB-CH$_2$py)** (CD_3CN) in the presence of 1 or 5 equiv. $HClO_4$ are overlaid, allowing us to identify the resonances of protonated pyridines and CH_2py protons. With 1 equiv. $HClO_4$, the macrocycle of **(cyclenCB-CH$_2$py)** is protonated. With 5 equiv., pyridine is also protonated.

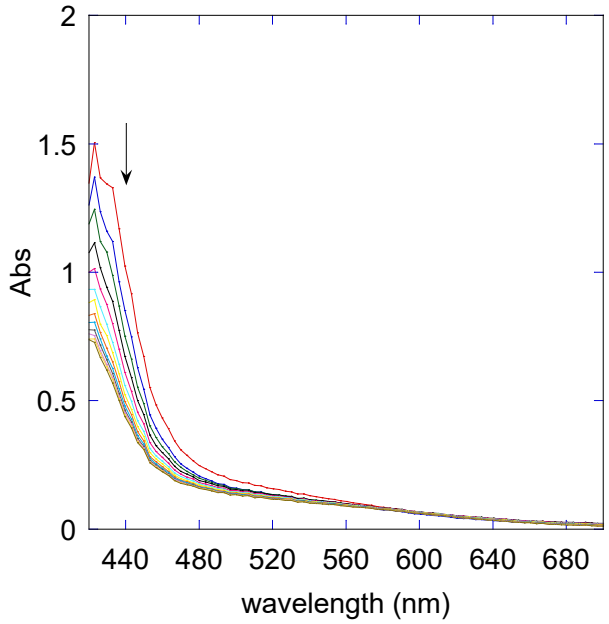

Figure S9. Change in absorbance of the UV-vis spectrum of **[(cyclenCB-CH$_2$py)Fe^{II}(OTf)](OTf)** after addition of 1 equiv. $HClO_4$ (MeCN, [Fe] = 1 mM, 20°C).

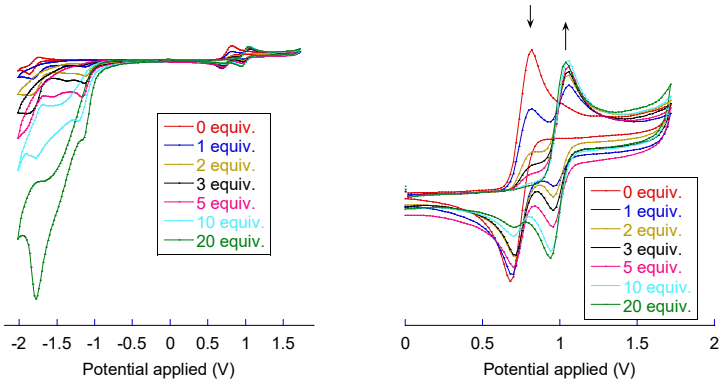

Figure S10. CV at a glassy carbon electrode of **[(cyclenCB-CH_2py)Fe^{II}(OTf)](OTf)** (C =2 mM) in MeCN (300 K) upon addition of $HClO_4$. NBu_4PF_6 0.1 M. WE: GC, CE: Pt, Ref: SCE. Couple at $E_{1/2}$ = 0.71 V (ΔE = 100 mV) *vs* SCE is ascribed to a $(N_5)Fe^{III}(MeCN)/(N_5)Fe^{II}(MeCN)$ couple and the one at at $E_{1/2}$ = 1.0 V (ΔE = 100 mV) *vs* SCE is ascribed to a $(N_4)Fe^{III}(MeCN)_2/(N_4)Fe^{II}(MeCN)_2$ couple resulting from the decoordination (protonation) of the pyridine. Note that a $(N_4)Fe^{III}(MeCN)(OH)/(N_4)Fe^{II}(MeCN)(OH)$ couple is expected to have $E_{1/2}$ around 0.7 V also (anion coordination induces a ca. 300 mV shift of the potential). the wave around 0.7 V on the reverse scan could thus also correspond to the reduction of a $(N_4)Fe^{III}(MeCN)(OH)$ complex.

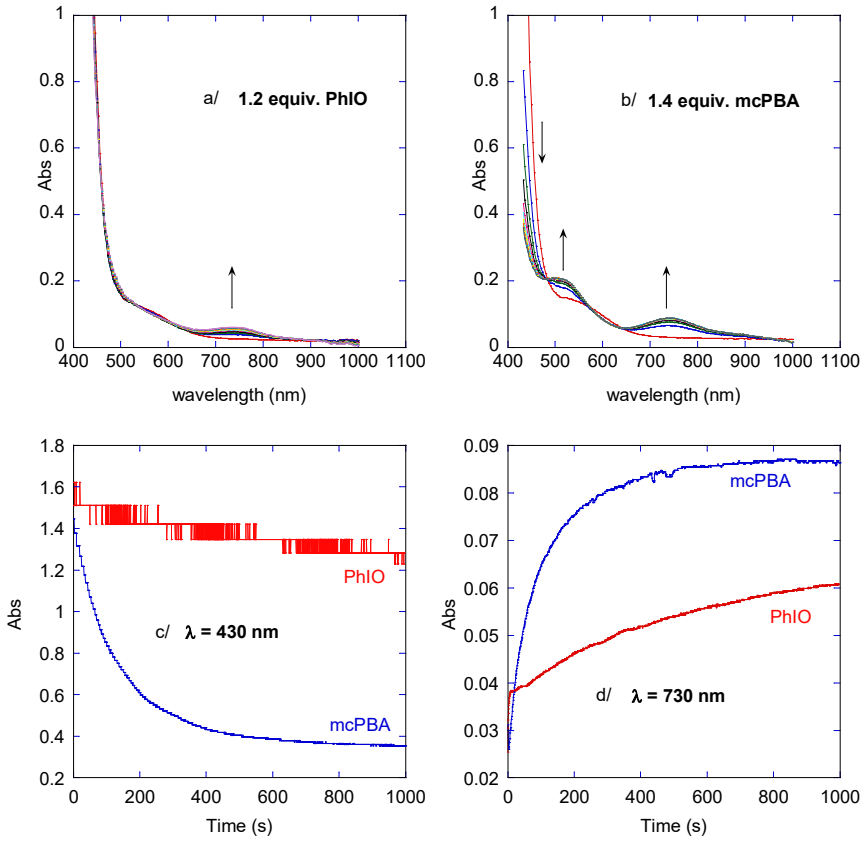

Figure S11. Evolution of the UV-vis sectrum of **[(cyclenCB-CH_2py)Fe^{II}(OTf)](OTf)** (C =1 mM) in MeCN (293 K), upon addition of 1.2 equiv. PhIO (a/) or 1.4 equiv. mCPBA (b/). Timetraces of the absorbances at 430 nm (c/) and 730 nm (d/) for these two experiments.

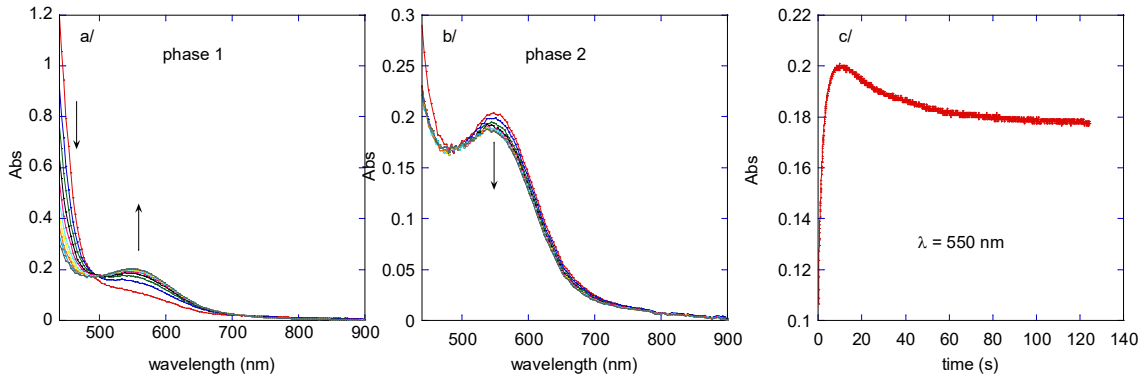

Figure S12. Evolution of the UV-vis spectrum of **[(cyclenCB-CH$_2$py)Fe^{II}(OTf)](OTf)** (C =1 mM) in MeCN (293 K), upon addition of 20 equiv. H_2O_2 : growth at 550 nm (phase 1, a/), decay at 550 nm (phase 2, b/) and timetrace at 550 nm (c/).

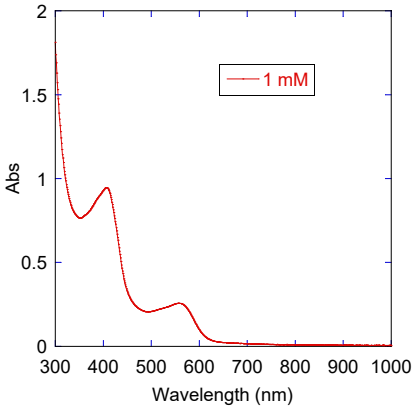

Figure S13. UV-vis spectrum of a solution of **[(cyclenCB-CH$_2$py)Fe^{II}(OTf)](OTf)** in MeCN ([Fe] = 1 mM, 0.1 M NBu_4PF_6, 293 K) oxidized by electrolysis.

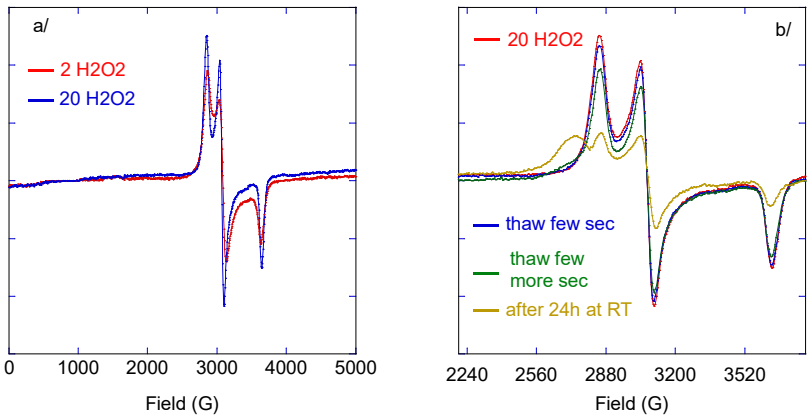

Figure S14. X-band EPR spectra (90 K) of the species accumulated upon mixing **[(cyclenCB-CH$_2$py)Fe^{II}(OTf)](OTf)** 1 mM in MeCN with 2 or 20 equ. H_2O_2 at 293 K after a 9 s delay (maximum of accumulation of the 550 nm chromophore, a/). Evolution of the X-band EPR spectra (90 K) of the **[(cyclenCB-CH$_2$py)Fe^{II}(OTf)](OTf)** / H_2O_2 1:20 mixture after successive thawing/freezing cycles (b/).

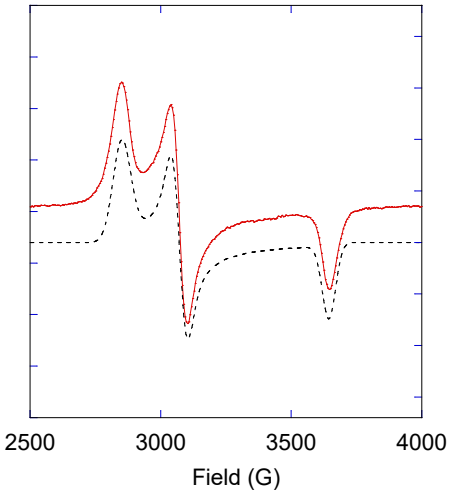

Figure S15. Low spin section of the X-band EPR spectra (90 K) of the species accumulated upon mixing **[(cyclenCB-CH_2py)Fe^{II}(OTf)](OTf)** 1 mM in MeCN with 20 equiv. H_2O_2 at 293 K after a 9 s delay (maximum of accumulation of the 550 nm chromophore, plain red line) and simulated spectrum (black dashed line) for a S=1/2 species with parameters g = 2.414 2.240 1.888.

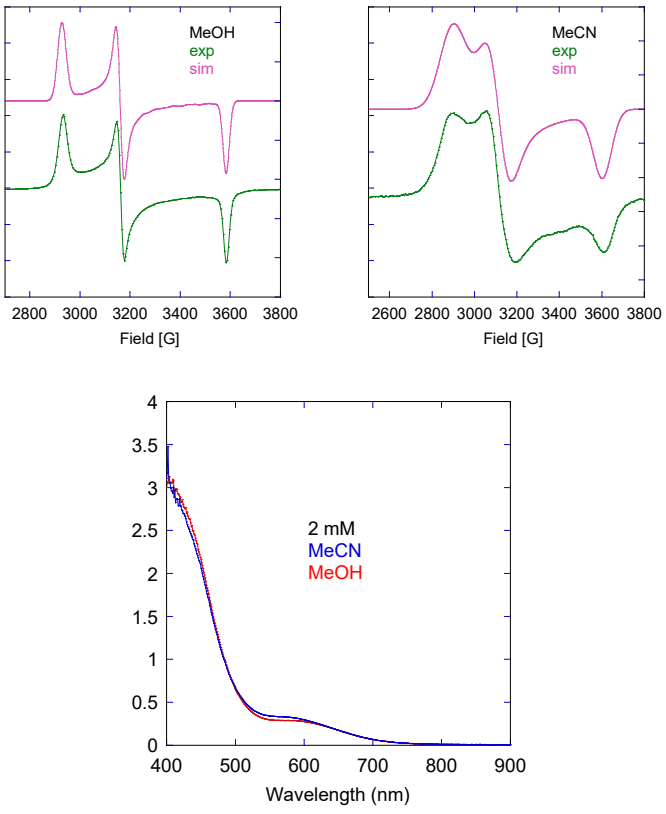

Figure S16. *Top:* X-band EPR spectra (90 K) of **[(cyclenCB-CH_2py)Fe^{III}(OMe)](OTf)$_2$** in MeOH (left) or MeCN (right) with corresponding simulations:g = 2.35, 2.18, 1.92 in MeOH; g = 2.38, 2.21, 1.91 in MeCN. The EPR signature is ascribed to [**(cyclenCB-CH_2py)Fe^{III}(OMe)]$^{2+}$**, the slight shift in the parameters being ascribed to the protic nature of methanol which can develop hydrogen bonds with the methoxo ligand, unlike MeCN. *Bottom:* UV-vis spectra of **[(cyclenCB-CH_2py)Fe^{III}(OMe)](OTf)$_2$** crystals in MeOH (red) or MeCN (blue) (293 K).

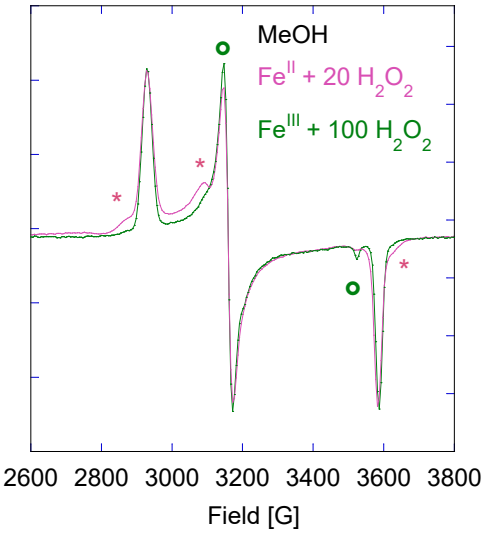

Figure S17. X-band EPR spectra (90 K) of **[(cyclenCB-CH_2py)Fe^{II}(OTf)](OTf)** in the presence of 20 equiv. H_2O_2 (pink) and **[(cyclenCB-CH_2py)Fe^{III}(OMe)](OTf)$_2$** in the presence of 100 equiv. H_2O_2 (green) in MeOH. The main species correspond to [**(cyclenCB-CH_2py)Fe^{III}(OMe)]$^{2+}$** . The pink stars indicate signals from [**(cyclenCB-CH_2py)Fe^{III}(OH)]$^{2+}$** and the green circles signals from **[(cyclenCB-CH_2py)Fe^{III}(OOH)]$^{2+}$**. The overall LS signal for the Fe(II) complex + 20 H_2O_2 represents around 70% of the Fe content. The LS signal for the Fe(III) complex + 100 H_2O_2 represents 75% of the Fe content.

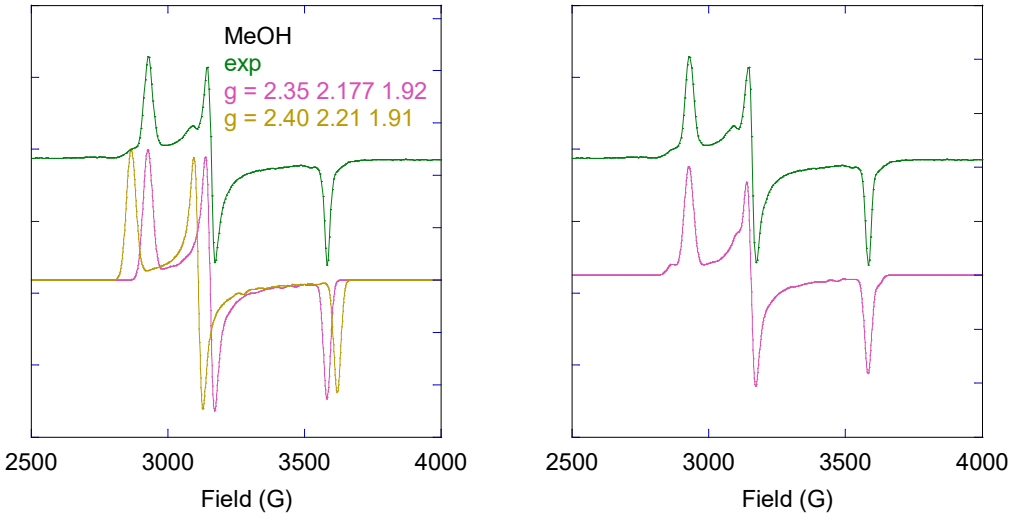

Figure S18. X-band EPR spectra (90 K) of **[(cyclenCB-CH_2py)Fe^{II}(OTf)](OTf)** in the presence of 20 equiv. H_2O_2 (green) in MeOH. (Left) With isolated simulations of A = (N_5)Fe^{III}(OMe) (g = 2.35 2.177 1.92) and B = (N_5)Fe^{III}(OH) (g = 2.40 2.21 1.91) and (Right) with the sum spectrum of both contributions (A + 0.1 B) (pink).

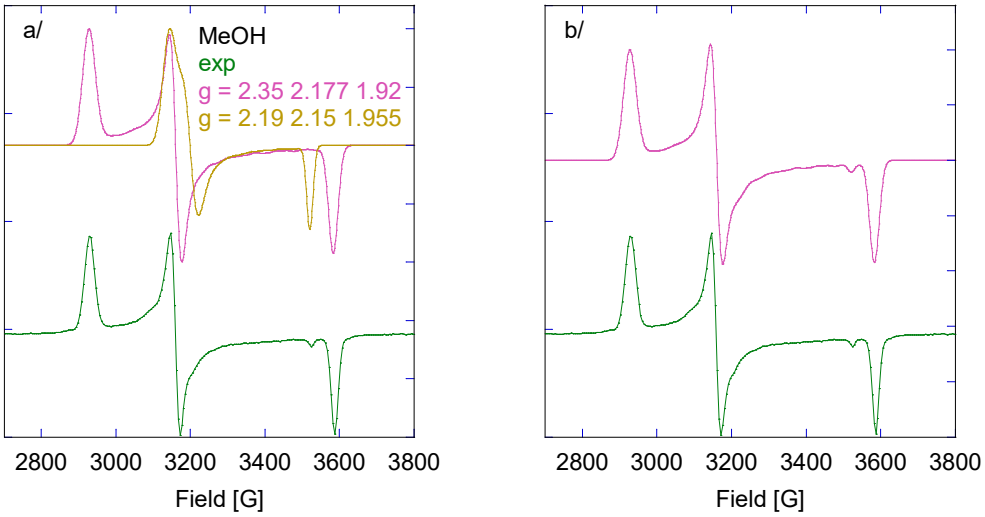

Figure S19. X-band EPR spectra (90 K) of **[(cyclenCB-CH_2py)Fe^{III}(OMe)](OTf)$_2$** in the presence of 100 equiv. H_2O_2 (green) in MeOH. With a/ isolated simulations of A = (N_5)Fe^{III}(OMe) (g = 2.35 2.177 1.92) and B = (N_5)Fe^{III}(OOH) (g = 2.19 2.15 1.955) and (b/) with the sum spectrum of both contributions (A + 0.1 B) (pink).

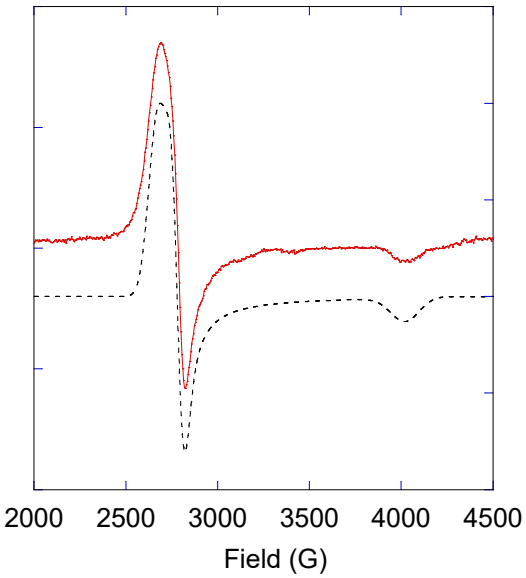

Figure S20. Low spin section of the X-band EPR spectra (90 K, MeCN) of the species accumulated upon addition of 1 equiv. $HClO_4$ to a **[(cyclenCB-CH_2py)Fe^{II}(OTf)](OTf)** / H_2O_2 1:20 mixture (plain red line) and simulated spectrum for a S =1/2 species with parameters g = 2.580, 2.475, 1.710. The overall LS signal represents around 72% of the Fe content.

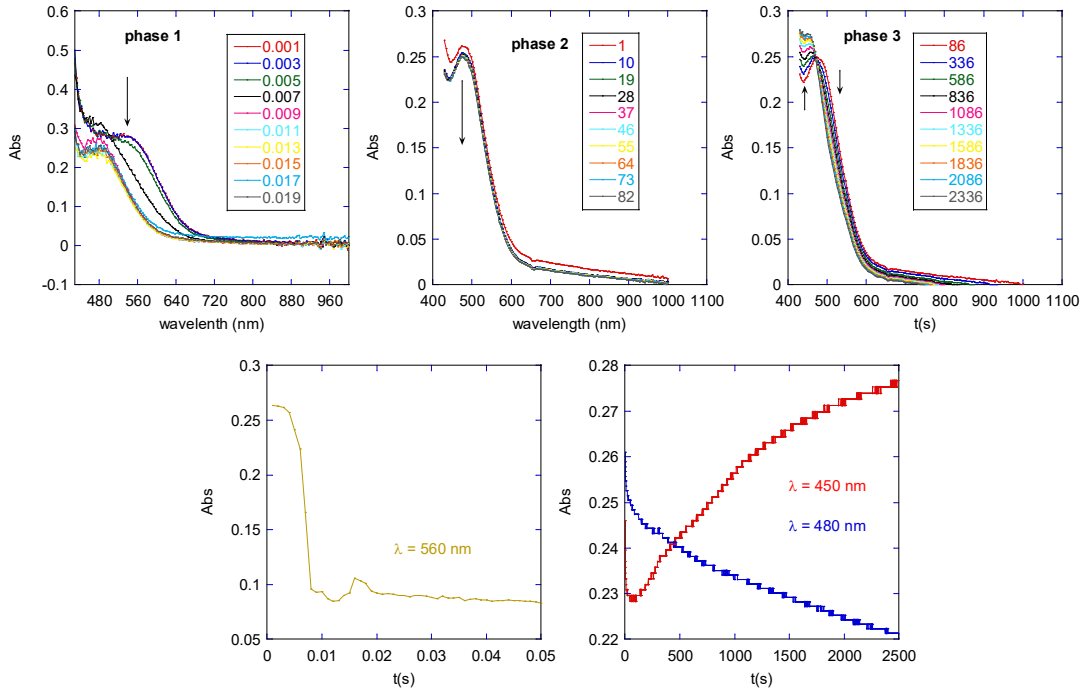

Figure S21. Evolution of the UV-vis spectrum (MeCN, 293 K, [Fe] = 1 mM) of a **[(cyclenCB-CH_2py)Fe^{II}(OTf)](OTf)** / H_2O_2 1:20 mixture solution (aged 9 s) upon addition of 1 equiv. $HClO_4$ (Top). Timetraces of the absorbances at 560, 480, and 450 nm (Bottom).

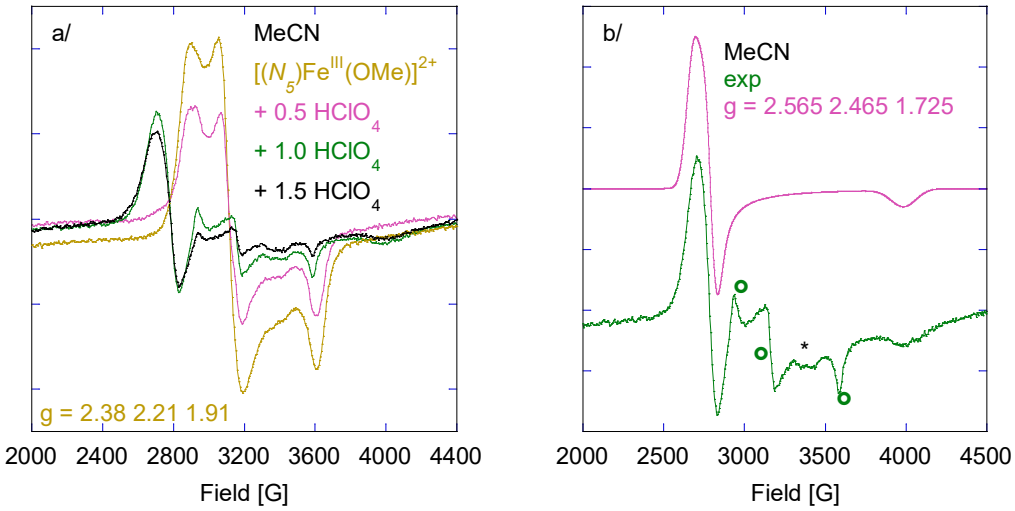

Figure S22. X-band EPR spectra (90 K) **[(cyclenCB-CH_2py)Fe^{III}(OMe)](OTf)$_2$** upon addition of different amounts of $HClO_4$ in MeCN (a/). Simulation of the EPR spectrum at the end of the titration with parameters g = 2.565 2.465 1.725 (b/). Green circles indicates the signals of remaining **[(cyclenCB-CH_2py)Fe^{III}(OMe)]$^{2+}$** and ***** a residual signal of the EPR cavity. The LS signal represents 97% of Fe content. Addition of 0.5 eq., 1 eq. and 1.5 eq $HClO_4$ lead respectively to LS signals representing 63, 58, 47 % of the Fe content respectively. After addition of H_2O_2 to this solution, it represents 42%.

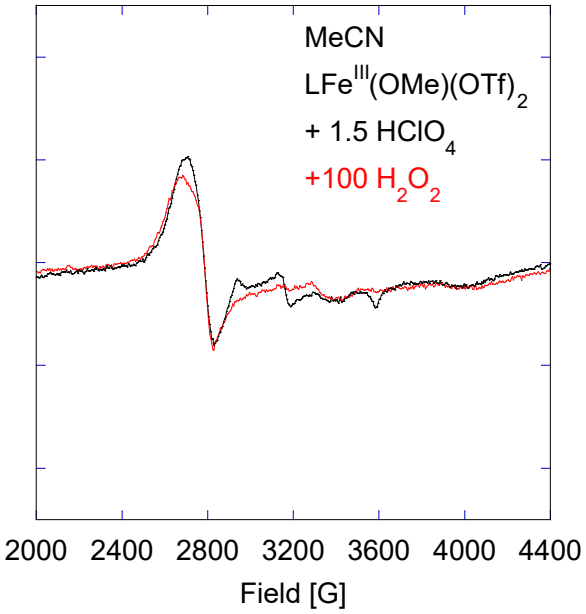

Figure S23. X-band EPR spectra (90 K) **[(cyclenCB-CH_2py)Fe^{III}(OMe)](OTf)$_2$** and 1.5 equiv. $HClO_4$ before (black) and after (red) addition of 100 eq. H_2O_2 in MeCN. The LS signal after addition of 1.5 eq $HClO_4$ represents 47 % of the Fe content. After addition of H_2O_2 to this solution, it represents 42% of the Fe content.

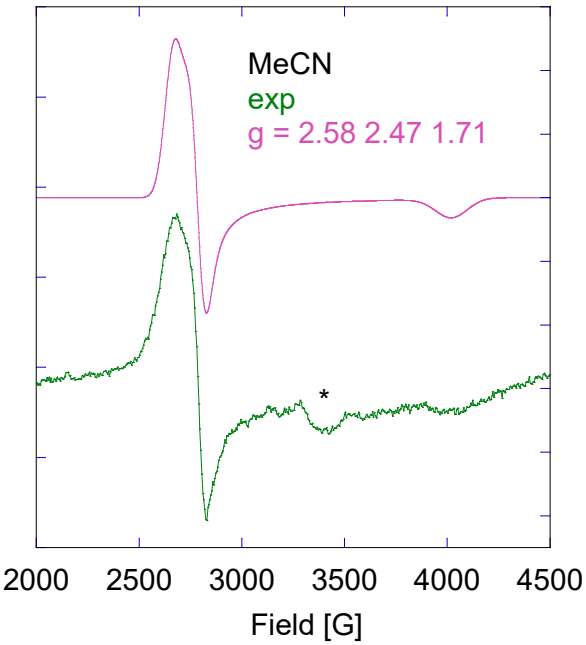

Figure S24. X-band EPR spectra (90 K) **[(cyclenCB-CH_2py)Fe^{III}(OMe)](OTf)$_2$** upon addition of 1.5 equiv. $HClO_4$ and 100 equiv. H_2O_2 in MeCN (green) and simulation (pink) with parameters g = 2.58 2.47 1.71. ***** a residual signal of the EPR cavity.

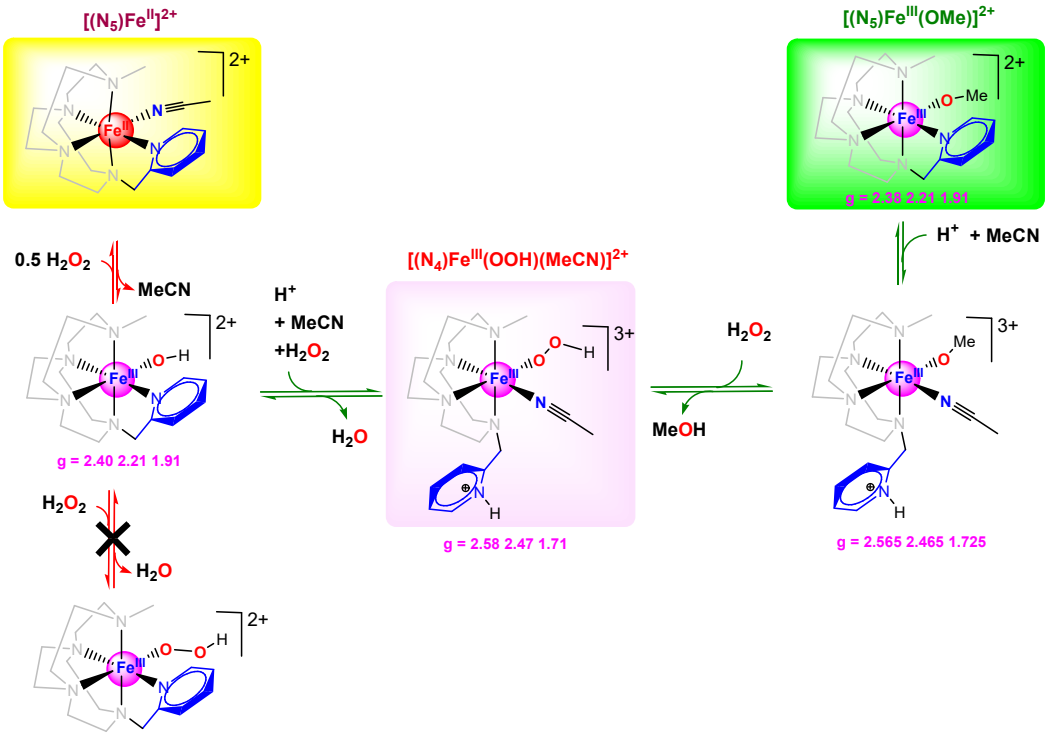

Scheme S1. Proposed steps for the formation of $[(N_4)Fe^{III}(OOH)]^{2+}$ from either $[(N_5)Fe^{II}(MeCN)]^{2+}$ or $[(N_5)Fe^{III}(OMe)]^{2+}$. g factors are indicated for species detected.

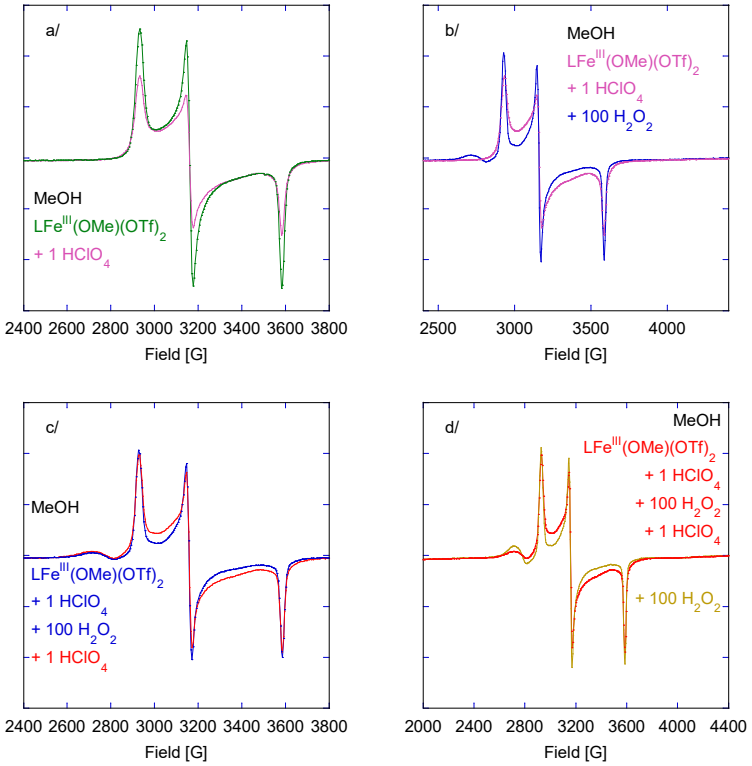

Figure S25. X-band EPR spectra (90 K) **[(cyclenCB-CH_2py)Fe^{III}(OMe)](OTf)$_2$** upon successive additions of $HClO_4$ and H_2O_2 in MeOH. The initial LS signal represents 75% of the Fe content. After addition of 1 eq.

$HClO_4$, it drops to 62 %. The first addition of H_2O_2 lowers it to 52%. Another aliquot of acid raises it to 66% and the second addition of H_2O_2 lowers it to 52%.

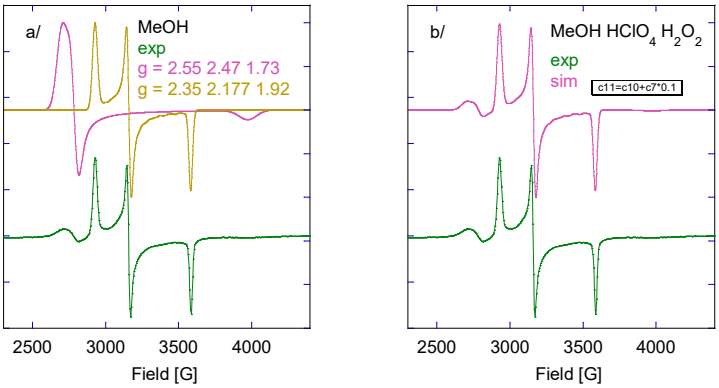

Figure S26. X-band EPR spectrum (90 K, MeOH) of a solution of **[(cyclenCB-CH_2py)Fe^{III}(OMe)](OTf)$_2$**, 2 equiv. $HClO_4$, and 200 equiv. H_2O_2, (green trace) and (a/) simulations (pink and yellow traces) with two sets of signals g = 2.55 2.47 1.73 ((N_4)Fe^{III}(OOH)(MeOH) = species A) and g = 2.35 2.177 1.92 ((N_5)Fe^{III}(OMe) = species B), and (b/) summed simulation of the two species (B + 0.1 A).

[1] K. R. Wilson, D. J. Cannon-Smith, B. P. Burke, O. C. Birdsong, S. J. Archibald, T. J. Hubin, *Polyhedron* **2016**, *114*, 118-127.

[2] G. M. Sheldrick, University of Göttingen, Germany, Göttingen, **1997**.

[3] G. M. Sheldrick, *Acta Crystallogr., Sect. A: Found. Crystallogr.* **2008**, *64* 112-122.

[4] L. J. Farrugia, *J. Appl. Cryst.* **1999**, *32*, 837.